Relationships of Propagated Error in Fraction of Vegetation Cover Among the Retrieval Algorithms Based on a Linear Mixture Model

Hiroki Yoshioka[a*], Kenta Obata[b]

Department of Information Science and Technology, Aichi Prefectural University, 1522-3 Kumabari, Nagakute, Aichi, Japan.
[a] yoshioka@ist.aichi-pu.ac.jp [b] kenta.obata@cis.aichi-pu.ac.jp

Abstract – Fraction of vegetation cover (FVC) is often estimated by unmixing a linear mixture model (LMM). In the LMM-based algorithm, differences can be seen in assumptions and constraints imposed to the model such as spectral vegetation index, inducing variations in algorithm. As a result, robustness against noises in reflectance spectrum is somewhat different among those algorithms, depending on a target spectrum to be analyzed, endmember spectra used for unmixing, and choice of two-band VI assumed in the algorithms. Objective of this study is to propose an analytical technique for better algorithm selection under a two-endmember assumption. Robustness against noises in reflectance spectrum is considered as a criterion. This criterion is first derived analytically, and then demonstrated numerically. It is shown that our proposing technique based on the derived factor is an indicator to determine a better algorithm against noises for any target spectrum over the entire red-NIR reflectance subspace.

Keywords: fraction of vegetation cover, linear mixture model, propagated error, optimum algorithm, vegetation index

1. INTRODUCTION

Several algorithms have been proposed to estimate fraction of vegetation cover (FVC) for subpixel-level estimation using remotely sensed reflectance spectrum (Guilfoyle, 2001; Xiao, 2005; Kallel, 2007). Unmixing a linear mixture model (LMM) is one of the most frequently used algorithms for FVC estimation (Smith, 1990). This study focuses on the one called LMM-based algorithm. The LMM-based algorithm shows variations itself due to differences in assumptions and constraints imposed to the models during the retrieval processes. These variations of the algorithm induce differences in FVC estimations from an identical reflectance spectrum. The relationships among FVCs by LMM-based algorithms have been investigated analytically under the two-endmember assumptions (Obata, 2010a). Although the relationship has been discussed analytically, comparison of their robustness against noises in reflectance spectrum has not been investigated within the analytical framework.

In practical application of the FVC algorithms, one encounters a decision making process regarding the algorithm choice. This type of decision is made mainly from accuracy point of view. For example, one approach is to conduct a set of numerical studies with numerical models and satellite data to determine accuracy in measuring FVC statistically. In this approach, some degree of uncertainty is always remained. While, in analytical approach, uncertainty can be treated separated from the comparison between two algorithms by assuming a certain error in a measured spectrum.

Reflectance spectrum observed by satellite sensor is deteriorated by various intervening factors such as instrumental noise, atmospheric contamination, and effect of background soil (Goward, 1991). Errors in a measured spectrum propagate to the FVC estimation, and this propagation process as well as its magnitude depends somewhat on the algorithms used/chosen. Information about the relationships between the propagated errors of different algorithms can be a basis of better algorithm selection. Obata and Yoshioka (Obata, 2010b) have derived the relationships between the propagated errors of different LMM-based algorithms analytically under the two-endmember assumption. This study is to step forward our previous work: We try to use the analytical expressions to determine a factor which becomes an indicator for algorithm selection.

Objective of this study is to propose a technique to compare the FVC retrieval algorithms in terms of propagated error. A criterion is derived analytically based on the derived expressions in our previous work. Below, we explain a derived factor of criterion after a brief theoretical background. Results of numerical experiments will be introduced to examine the derived criterion.

2. BACKGROUND

The LMM-based algorithms under the two-endmember assumption can be categorized into three on the conditions/constraints used in the algorithms. Details of the LMM-based algorithms and differences among those were discussed in (Obata, 2010a). In this study, we denote three algorithms, reflectance-based LMM, vegetation index-based LMM, and isoline-based LMM, as algorithm-1, -2, and -3, respectively. Errors in a reflectance spectrum propagated into FVC value by the three algorithms, represented by ε_1, ε_2, and ε_3, are derived as a function of a target spectrum, a band-correlated noise, endmember spectra, and choice of two-band

* Corresponding author

** This work was supported by JSPS KAKENHI 21510019 (HY) and the Nitto Foundation (KO).

vegetation index (VI) used as conditions in algorithm-2 and -3 (Obata, 2010b). Below, those factors are expressed simply as 'input data'. Relations between any two pair of the propagated errors (ε_1 , ε_2 , and ε_3) can be written by the fallowing expression (Obata, 2010b) as

$$\sum_{i=0}^{2}\sum_{j=0}^{2} p_{i,j} x^i y^j = 0, \tag{1}$$

where x^i and y^j are any pair of ε_1 , ε_2 , and ε_3 . The coefficients $p_{i,j}$ are defined by the input data. The formulations and coefficients for each algorithm had been explained precisely in our previous work (Obata, 2010b). The relationship by any pair of the propagated error (ε_1 , ε_2 , and ε_3) becomes an asymmetric ellipse as shown in Fig. 1. The length and slope of the major and minor axes in the ellipse depend on the input data. A certain point in the ellipse is determined by the direction of the band-correlated noise over the red-NIR reflectance subspace.

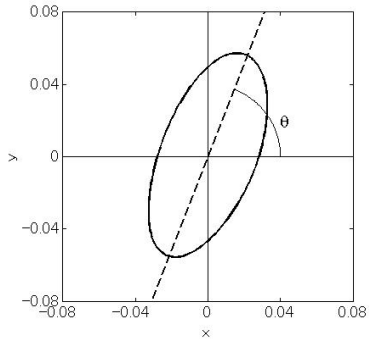

Figure 1. Relationship of the propagated errors in FVC among LMM-based algorithms. The angle (the slope) of a major axis of the ellipse is denoted by θ . If the slope ($\tan\theta$) is larger than one, the algorithm assigned for x -axis is superior to the algorithm for y -axis.

3. METHOD

Our focus is the derivation of the slope of the major axis in the asymmetric ellipse (Fig. 1) that indicates superiority in robustness between two algorithms. When the slope is larger than unity, average of y-value is relatively larger than that of x-value. It implies that the error assigned as y-axis tends to be larger than the one assigned as x-axis, meaning that that algorithm of x is superior to that of y axis. It becomes vice versa when the slope is lower than unity. The slope can be expressed by the angle θ as a function of the coefficients $p_{i,j}$ in Eq. (1), as

$$\theta \approx \frac{1}{2}\tan^{-1}\frac{p_{1,1}}{p_{2,0} - p_{0,2}}, \tag{2}$$

where the coefficients $p_{2,0}$, $p_{0,2}$ and $p_{1,1}$ depend on the choices of the algorithms assigned for x and y values. The definitions of those coefficients for each pair of the algorithms were summarized in (Obata, 2010b). Equation (2) approximates the slope of the major axis in the asymmetric ellipse, obtaining by neglecting the effect of higher order terms in Eq. (1). Note that those coefficients are mainly determined by the three factors of the input data: those are 1) target spectrum, 2) endmember spectra, and 3) choice of VI used in the algorithm as a condition/constraint. It means that, if a target field (target spectrum) and assumptions in the algorithms (endmember spectra) were fixed, superiority among the algorithms will be determined without intensive parameter studies.

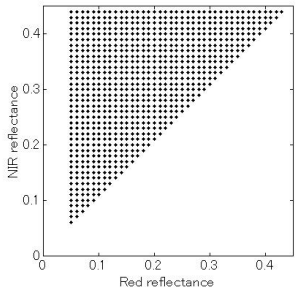

Figure 2. Target spectra in the red-NIR reflectance subspace.

4. NUMERICAL VALIDATION

In this section we examine our proposing technique to compare the algorithms based on the derived factor, Eq. (2). Since the factor depends on a target spectrum, the comparison was made for the various target spectra over the region in red-NIR reflectance space as shown in Fig. 2. We consider two sets of endmember spectra. One is a pair of (0.05, 0.4) and (0.1, 0.1) for the vegetation and non-vegetation endmember spectra, respectively, denoted as EM1. The other is a pair of (0.05, 0.4) and (0.3, 0.3) for the endmember spectra, denoted as EM2. We assumed NDVI, SAVI and EVI2 as a constraint in the algorithm. The magnitude of the noise spectrum in the reflectance is assumed to be 0.01 as a distance from a target spectrum.

The variable $\tan\theta$ is calculated for each target spectrum for the pairs of the LMM-based algorithms under two sets of endmember spectra. The variable $\tan\theta$ is plotted in logarithmic scale as contour plot in red-NIR reflectance subspace (Figs. 3-7). The pair of the algorithm evaluated in the simulations is also denoted in each figure such as 'A vs. B'. When $\log(\tan\theta)$ is larger than zero ($\tan\theta$ is larger than one), algorithm-A is

considered to be better than algorithm-B regarding the propagated noise in FVC estimation. Figure 3 is the comparison between algorithm-1 and 2, and algorithm-1 and 3 using three different VIs as a constraint with the endmember set of EM1. Figures 4 is the same comparison with the endmember set of EM2. Figures 5 and 6 are the comparisons between algorithm-2 and 3 as Figs. 3 and 4, respectively. Finally, Fig. 7 shows the comparison between algorithm-2 and 3 for both endmember cases.

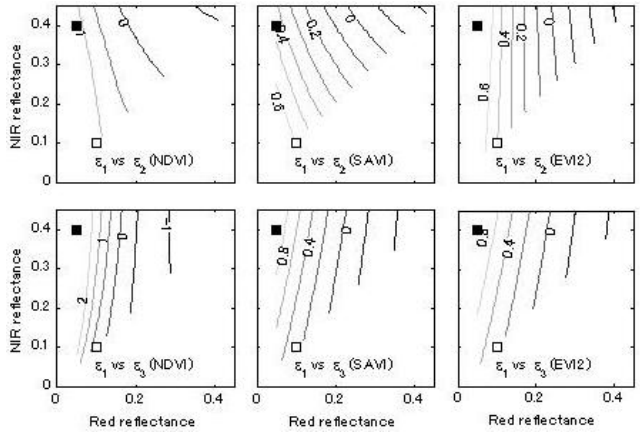

Figure 3. Contour plot of the slope, $\tan\theta$ in log scale over red-NIR reflectance space for evaluating the superiority between algorithm-1 and -2, and between algorithm-1 and -3 assuming EM1 as the endmember spectra.

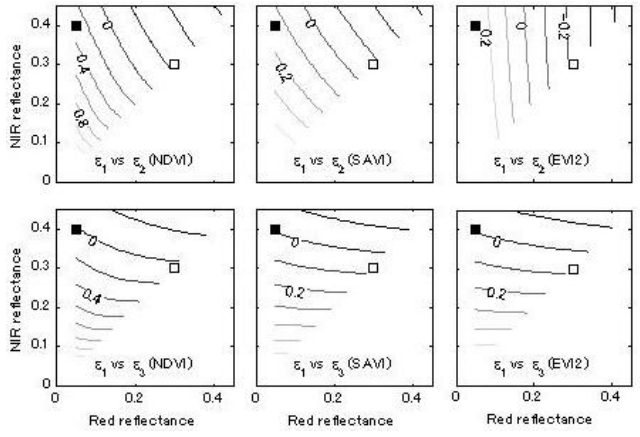

Figure 4. Contour plot of the slope, $\tan\theta$ in log scale obtained by altering endmember spectra from EM1 to EM2 for the results in Fig. 3.

Overall, these figures indicate strong dependency of $\tan\theta$ on the target spectrum, the choice of endmember spectra, and VI used in the algorithm. In the figures, note that the contour line for $\log(\tan\theta)=0$ is the boundary along which the two algorithms (in comparison) would show nearly the same pattern and magnitude of the propagated error, meaning that the two algorithms would show no difference in terms of the propagated errors in FVC values. From upper left figure in Fig. 3, for example, $\log(\tan\theta)$ is greater than zero for lower value of red reflectance, meaning that ε_1 is mostly smaller than ε_2. For those target spectra, algorithm-2 is better than algorithm-1 regarding the propagated error.

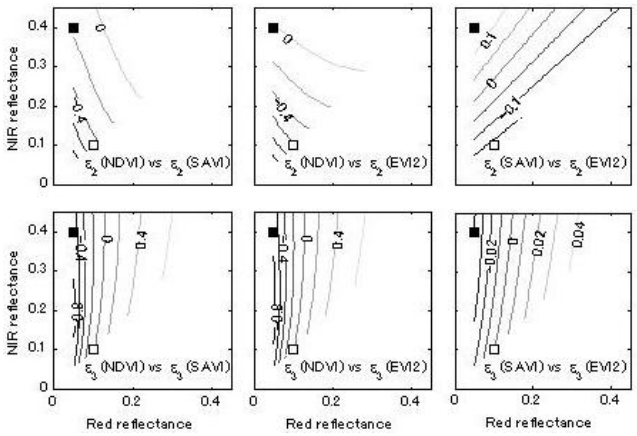

Figure 5. Contour plot of the slope, $\tan\theta$ in log scale over red-NIR reflectance space for evaluating the superiority among algorithm-2 using different VIs, and among algorithms-3 using different VIs based on EM1 as the endmember spectra.

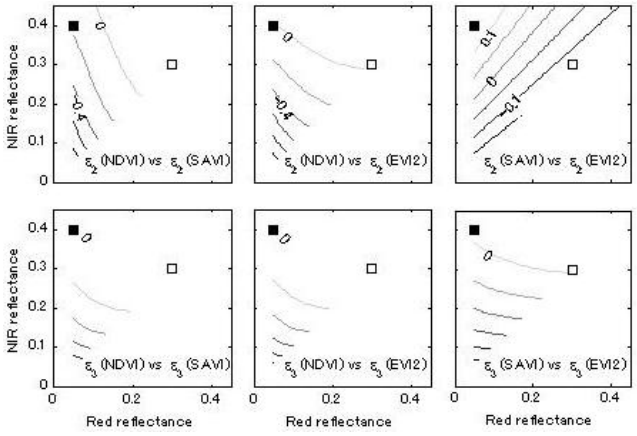

Figure 6. Contour plot of the slope, $\tan\theta$ in log scale obtained by altering endmember spectra from EM1 to EM2 for the results in Fig. 5.

Dependencies of target spectrum and two-band VI can be clearly seen, for example, in Fig. 3. Dependencies of endmember spectra on θ can also be seen by comparing Figs. 3 and 4 (results obtained by altering EM1 to EM2). Especially, contour lines of

$\log(\tan\theta)$ in lower three (comparison between algorithm-1 and algorithm-3) in Fig. 3 align vertically, while, those in Fig. 4 align horizontally. From those figures, algorithm-1 would be more robust than algorithm-2 or –3 for the darker target.

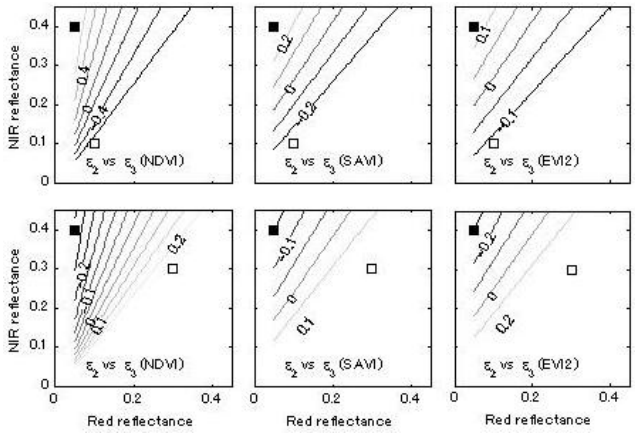

Figure 7. Contour plot of the slope, $\tan\theta$ in log scale over red-NIR reflectance space for evaluation of the superiority between algorithm-2 and -3, using the same two-band VI assuming EM1 (upper three) and EM2 (lower three).

Results of $\log(\tan\theta)$ for algorithm-2 or -3 using different type of VI are shown in Figs. 5 (using EM1) and 6 (using EM2). Endmember effect is clearly observed in results of algorithm-3. On the other hand, the variation of endmember spectrum has small influence on the comparison within algorithm-2. Those results might infer the fact that FVC computed by algorithm-3 depends relatively larger on endmember spectra comparing to that by algorithm-2. Magnitude of θ is also different among the pairs of VI, although $\log(\tan\theta)$ -isoline (contour) shows similar pattern for those cases with only exception of the upper right plot in Figs. 5 and 6.

Figure 7 shows the comparison between algorithm-2 and -3 using the same VI with two sets of endmember spectra. Upper three are for EM1, and lower three are for EM2. All the patters of $\log(\tan\theta)$ -contour are similar, indicating the similarity in their behaviors against the error. Endmember spectra (non-vegetation) has small influence on the contour pattern. In addition, from the contour pattern, when the VI value of the target spectrum is lower, algorithm-2 is more robust against the errors. When the VI value becomes higher, it turns out that algorithm-3 becomes a better choice.

5. REMARKS

We introduced a technique to compare the FVC retrieval algorithms regarding the robustness against error in a reflectance spectrum which is eventually propagated into the FVC value. We derived a factor as an indicator of the robustness, which is defined by endmember spectra, coefficients of the VI model equation assumed in the algorithm, and reflectance spectrum of a target pixel. Once an average target spectrum endmember spectra are fixed, those algorithm can be compared deterministically. Thus, based on this factor, we can avoid statistical analysis by conducting an intensive parameter study with numerical models and field data.

In this study we limit both the number of endmember spectra and the number of bands into two to facilitate the analytical approach. Although those assumptions may be unrealistic in practical application, the introduced technique would help to understand fundamental differences, which provides rich information for selecting the optimum algorithm for individual target field.

REFERENCES

S.N. Goward, B. Markham, D.G. Dye, W. Dulaney, and J. Yang, "Normalized difference vegetation index measurements from the advanced very high resolution radiometer," Remote Sens. Environ., vol. 35, p.p. 257-277, 1991.

K.J. Guilfoyle, M.L. Althouse, and C. Chein-I, "A quantitative and comparative analysis of linear and nonlinear spectral mixture models using radial basis function neural networks," IEEE Trans. Geosci. Remote Sens., vol. 39, p.p. 2314-2318, 2001.

A. Kallel, S.L. Hearat-Mascle, C. Ottle, and L. Hubert-Moy, "Determination of vegetation cover fraction by inversion of a four-parameter model based on isoline parameterization," Remote Sens. Environ., vol. 111, p.p. 552-566, 2007.

K. Obata and H. Yoshioka, "Inter-Algorithm Relationships for the Estimation of the Fraction of Vegetation Cover Based on a Two Endmember Linear Mixture Model with the VI Constraint," Remte Sens., vol. 2, p.p. 1680-1701, 2010a.

K. Obata and H. Yoshioka, "Relationships Between Errors Propagated in Fraction of Vegetation Cover by Algorithms Based on a Two-Endmember Linear Mixture Model," Remote Sens., vol. 2, p.p. 2680-2699, 2010b.

M.S. Smith, S.L. Ustin, J.B. Adams, and A.R. Gillespie, "Vegetation in deserts: I. A regional measure of abundance from multispectral images," Remote Sens. Environ., vol. 31, p.p. 1-26, 1990

J. Xiao and A. Moody, "A comparison of methods for estimating fractional green cover within a desert-to-upland transition zone in central New Mexico, USA," Remote Sens. Environ., vol. 98, p.p. 237-250, 2005.